High electrochemical performance of hybrid cobalt oxyhydroxide/nickel foam graphene

Tshifhiwa M. Masikhwa, Moshawe J. Madito, Damilola Momodu, Abdulhakeem Bello, Julien K. Dangbegnon, and Ncholu Manyala*

Department of Physics, Institute of Applied Materials, SARCHI Chair in Carbon Technology and Materials, University of Pretoria, Pretoria 0028, South Africa.

* Corresponding author: E-mail: ncholu.manyala@up.ac.za (N.Manyala), Tel: +27 (0)12 420 3549; Fax: +27 (0)12 420 2516.

ABSTRACT

In this study, we report the in-situ hydrothermal synthesis of mesoporous nanosheets of cobalt oxyhydroxide (CoOOH) on nickel foam graphene (Ni-FG) substrate, obtained via atmospheric pressure chemical vapour deposition (AP-CVD). The produced composite were closely interlinked with Ni-FG, which enhances the synergistic effect between graphene and the metal hydroxide, CoOOH. It is motivating that the synthesized CoOOH on the Ni-FG substrate showed a homogenous coating of well-ordered intersected nanosheets with porous structure. The electrochemical properties of the material as electrode showed a maximum specific capacity of 199 mAh g^{-1} with a capacity retention of 98% after 1000 cycling in a three electrode measurements.

Keywords: Cobalt oxyhydroxide, graphene foam, Ni-foam graphene, hybrid electrode, CoAl-LDH.

1. Introduction

Recently, research on electrode materials for supercapacitor applications has become one of the most important research topics in energy storage materials. Supercapacitor has received much attention due to its advantages of long cycle life, moderate specific energy density (~10 Wh kg^{-1}), high power density (>10 kW kg^{-1}) and short charging time [1–3]. These characteristics meet the increasing demand for power tools, hybrid electric vehicles and time-dependent electric power systems for portable electronics [4]. In the supercapacitor, the electrode material plays a significant role in the electrochemical capacitive performance. In the last decades, different types of electrode materials have been used in supercapacitor including carbonaceous materials, transitional metal hydroxides/oxide and conducting polymers [1,2,5,6]. Amongst these transitional metals, hydroxides/oxides have received much attention for high-performance due to their high specific capacitances, low costs, low toxicity, great flexibility in structure and morphology [7–14].

In addition, the cobalt oxyhdroxide is an improved charge storage material due to its morphology control nature of micrometer/nanometer scale and reasonably lower material costs[15,16]. However cobalt oxyhdroxide practical capacitance is less than 200 Fg^{-1} due to its low conductivity [17]. To improve the ionic transportation and electrical conductivity, various metal nanostructures and composites combined with carbon materials such as activated carbon, conducting polymers and graphene, with high surface area and high conductivity have been studied [18–22]. Among these materials, a porous and light-weight, graphene foam material (i.e. 3D structured graphene from nickel form templates) has been studied extensively as an ideal matrix for the growth of metal nanostructures because of its high conductivity [23–26]. Different kinds of nanostructured metal hydroxides/oxides have been deposited on graphene foam (GF) electrodes for supercapacitor applications [27,28]. For instance, Zhu *et al.* [9] considered Cobalt oxide (CoO) nanorods cluster on three-dimensional

graphene(CoO-3DG) through a facile hydrothermal method followed by heat treatment which improved electrochemical capacitive performance, Dong *et al* also produced 3D graphene/CO_3O_4 nanowire composites which demonstrated remarkable performance in supercapacitor [29], Zhao *et al* synthesized $Co(OH)_2$/graphene/Ni foam nano electrodes with high cycling stability for supercapacitor [30], Nguyen et al also reported 3D CO_3O_4/graphene/nickel foam with enhanced electrochemical performance for supercapacitor [31] and Deng *et al.* [32] synthesized CoO composited with 3D GF through a combination of hydrothermal method and thermal treatment which exhibited a high specific capacitance, excellent rate capability, and cycling stability as electrode material.

In this study, mesoporous nanosheets of cobalt oxyhydroxide (CoOOH) were synthesized on Ni foam graphene (Ni-FG) substrate by facile two-step processes, namely, hydrothermal reaction to produce CoAl-LDH nanosheets on Ni-FG which were converted to CoOOH nanosheets on Ni-FG by alkaline etching of the Al cations in CoAl-LDH using a NaOH solution. The CoOOH/Ni-FG electrode showed the specific capacity of 95 mAh g^{-1} at 10.0 A g^{-1} with 98 % capacity retention after 1000 cycles.

2. Experimental details

2.1 Graphene growth on nickel foam using AP-CVD

A Ni foam graphene substrate was synthesized by growing graphene sheets on the polycrystalline Ni foam (3D scaffold template with a macroporous structure) using atmospheric pressure chemical vapour deposition (AP-CVD). Polycrystalline Ni foam (Ni-F) (3D scaffold template with a macroporous structure) with an areal density of 420 g m^{-2} and 1.6 mm in thickness, was used as a substrate for graphene growth. A piece of Ni-F (2 cm × 3 cm) was treated with dilute hydrochloric acid, ethanol and distilled water to clean the surface of the foam. A cleaned Ni-F was placed at a centre of a quartz tube for graphene growth and

was annealed at 1000 °C under Ar and H_2 gases for 60 min and graphene was synthesized from a mixture of Ar: H_2: CH_4 (300: 200: 10 sccm respectively) gases at a temperature of 1000 C for 10 min. Immediately after 10 min, the CH_4 flow was stopped and samples were rapidly cooled down (under Ar and H_2 gases) by pushing the quartz tube to the cooler region of the furnace. At less than 80 ^{0}C, Ni-F graphene was off loaded from AP-CVD quartz tube. A synthesized Ni foam graphene (Ni-FG) substrate was further used for growth of CoOOH nanosheets.

2.2 CoOOH growth on Ni foam graphene (Ni-FG) using hydrothermal method

CoOOH nanosheets supported on nickel foam graphene were deduced from in-situ hydrothermally prepared CoAl-LDH on Ni-FG substrate by alkaline etching in concentrated NaOH solution as reported in ref [33]. A solution (pink in colour) for hydrothermal reaction was prepared by adding Co $(NO)_3$. $6H_2O$ (2 mmol), Al $(NO_3)_3.6H_2O$ (2 mmol), NH_4F (8 mmol) and CO $(NH_2)_2$ (10 mmol) in 36 mL of deionized water and stirred for 10 min, as demonstrated in figure 1. Ni-FG substrate was immersed into the above solution and then carefully transferred into a sealed Teflon-lined stainless-steel autoclave and kept at a temperature of 100°C for 24 h (figure 1). After cooling of an autoclave to room temperature, the obtained CoAl-LDH coated on Ni-FG was cleaned with dionized water. Then, the CoAl-LDH coated Ni-FG was immersed in 5 mol L^{-1} NaOH for 48 h and subsequently rinsed with deionized water, followed by ethanol for 5 min using ultrasonic bath, and dried at 60 °C for 6 h to obtain the final product CoOOH nanosheets (shown by micrograph image in the last step of figure 1) on Ni-FG substrate. The weight of the CoOOH film on Ni-FG substrate was measured by weighing the Ni-FG substrate before and after hydrothermal process, and a mass loading of ~5 mg cm^{-2} was obtained.

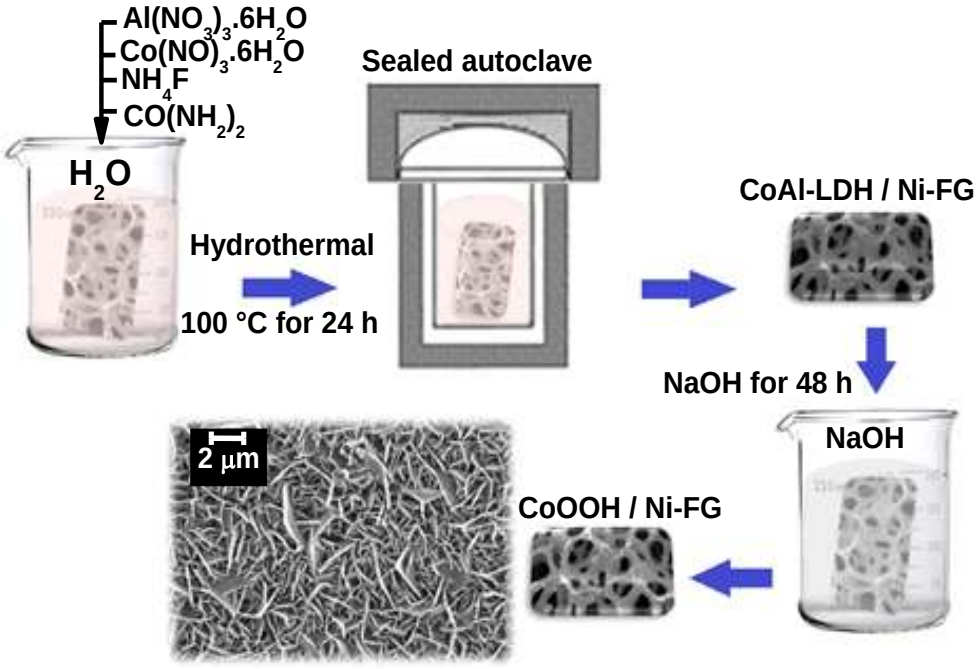

Figure 1: A schematic view of the hydrothermal growth of CoAL−LDH on graphene synthesized on Ni foam and alkaline etching in concentrated NaOH solution which produces a mesoporous structure of CoOOH on Ni foam graphene.

3. Materials characterizations

The as-prepared Ni-FG and CoOOH film on Ni-FG were characterized by X-ray diffraction (XRD) using a XPERT-PRO diffractometer (PANalytical BV, Netherlands) with theta/2 theta geometry, operating with a Co Kα radiation source (λ = 1.789 Å). The XRD spectra were acquired at a scanning rate of 0.2 s^{-1} and 2θ range of 15 to 70^0. Raman spectroscopy measurements were carried out using WITec Alpha 300 micro-Raman system with 532 nm excitation laser. Raman spectra were measured at room temperature with the laser power set below 5 mW in order to minimize heating effects. The SEM images were obtained on a Zeiss Ultra Plus 55 field emission scanning electron microscope (FE-SEM) operated at 2 kV beam and the working distance (WD) of 2.7 mm. The FE-SEM is equipped with an energy-dispersive X-ray spectrometer (EDX).

4. Electrode preparation and electrochemical characterization

The performance of Ni-FG and CoOOH film on Ni-FG were investigated using a Bio-Logic VMP300 potentiostat (Knoxville TN 37,930, USA) controlled by the EC-Lab® V10.40 software in a three-electrode configuration. The Ni-FG or CoOOH/Ni-FG (1 cm × 2 cm) served as the working electrode in a 6 M potassium hydroxide (KOH) electrolyte; glassy carbon plate was used as the counter electrode and Ag/AgCl (3 M KCl) as the reference electrode. The cyclic voltammetry (CV) tests were carried out in the potential range of 0 to 0.45 V (vs. Ag/AgCl) at different scan rates ranging from 5 to 50 mV s^{-1}. The galvanostatic charge-discharge (GCD) measurements were performed at various current densities from 0.5 to 10 A g^{-1} and the electrochemical impedance spectroscopy (EIS) measurements were performed in the frequency range of 10 mHz to 100 kHz.

5. Results and discussion

5.1 Morphology and structure

Figure 2 (a) and (b) show the XRD patterns of the Ni-FG substrate and CoOOH on the Ni-FG substrate and the corresponding JCPDS files. The XRD patterns show poor intensities diffraction peaks (the intensities are embedded in the signal noise level) of CoOOH at diffraction angles of 23.5 , 45.5 and 59.5 relative to the high intensities diffraction peaks of the Ni-FG substrate marked with "*" (figure 2 (b)).

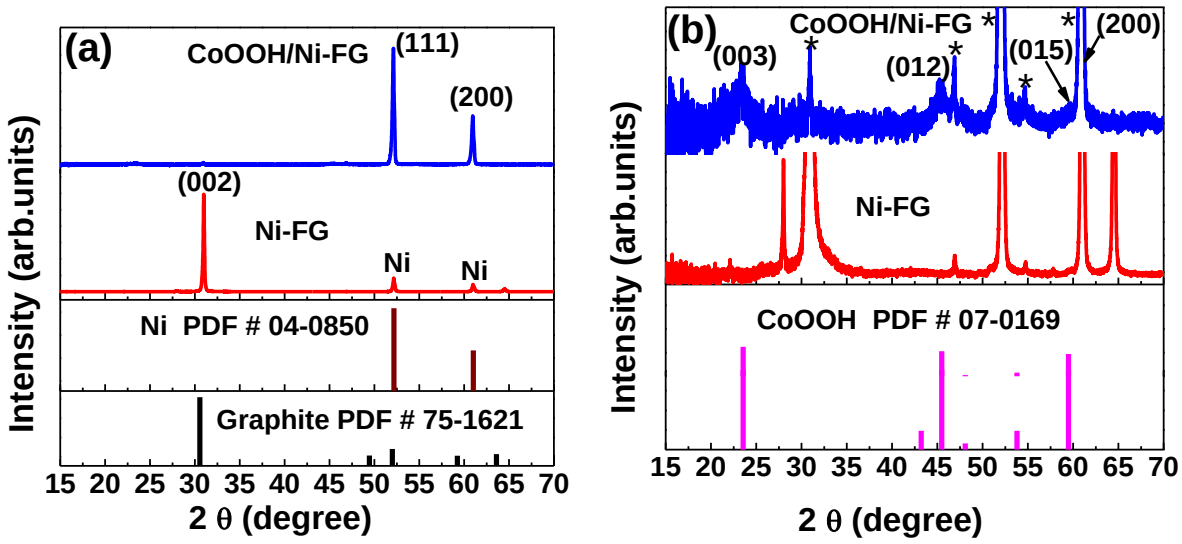

Figure 2: (a) and (b) XRD patterns of the Ni-FG substrate and CoOOH on the Ni-FG substrate and the corresponding JCPDS files.

The XRD patterns of the Ni-FG substrate and CoOOH on the Ni-FG substrate shown in figure 2 (a) and (b) were indexed using the graphite JCPDS card: 75-1621 (Sys: hexagonal, S.G.: P63mc (186), *a*: 2.470 Å, *c*: 6.790 Å), Ni JCPDS card: 04-0850 (Sys: cubic, S.G.: Fm3m (225), *a*: 3.523 Å) and CoOOH JCPDS card: 07-0169 (Sys: hexagonal, S.G.: R3m (166), *a*: 2.855 Å, *c*: 13.15 Å). The XRD data suggest that CoOOH synthesized on Ni-FG substrate has a hexagonal crystal structure similar to that of graphene.

Figure 3 (a) shows the Raman spectra of the CoOOH/Ni-FG and Ni-FG and the peaks observed at 1587 and 2701 cm^{-1} corresponds to the G-band and 2D-band modes of graphene and the other peaks to CoOOH compound. The absence (low-intensity) of the disorder-induced D-band at ~1350 cm^{-1} confirms the high-quality of graphene sheet [34–36]. The synthesized graphene sheet has a non-uniform thickness (varying between 1 to few graphene layers) over the entire Ni foam since polycrystalline Ni typically grows multilayer graphene sheets with varying thickness due to non-uniform precipitation of carbon atoms from different grains surfaces and grain boundaries [37–39]. Figure 3 (b) shows peaks of CoOOH

compound as shown in figure 3 (a) and the peaks were fitted with peaks at 506, 572, 632, 700, 1033, 1068 and 1165 cm^{-1} assigned to the CoOOH crystalline compound. These peaks positions correspond to the values published by Yang *et al.* [40] and Pauporte *et al.* [41] for Raman spectra of the CoOOH compound. Bands fittings were done using a Lorentz function and the fittings were carried out until reproducible fitting was obtained with squared correlation, r^2 of 0.99.

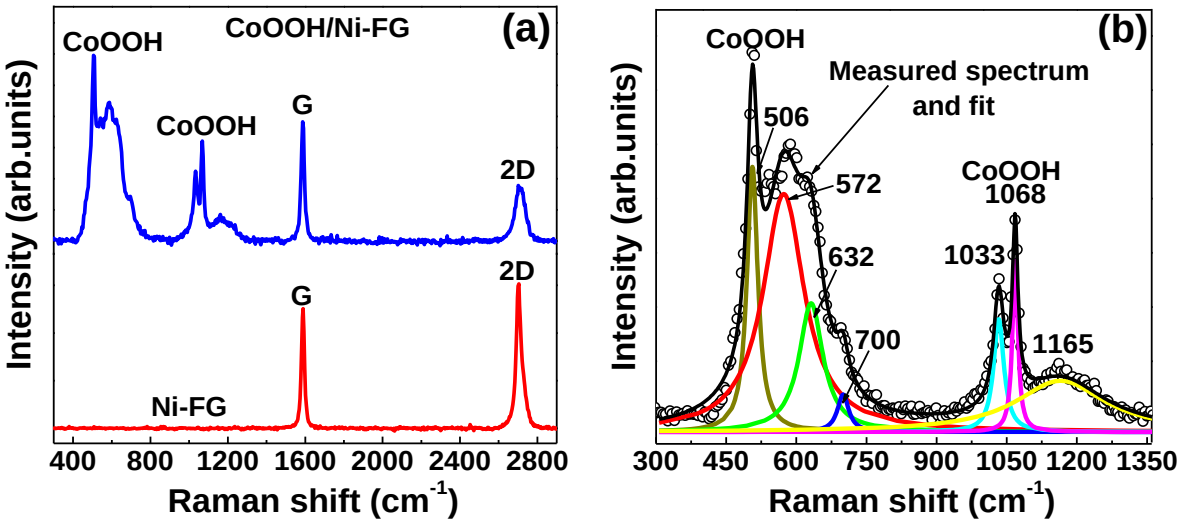

Figure 3: (a) Raman spectra of the CoOOH synthesized on the Ni-FG substrate (CoOOH/Ni-FG) and that of the graphene sheet on the Ni foam (Ni-FG). (b) Lorentz fittings of peaks at 506, 572, 632, 700, 1033, 1068 and 1165 cm^{-1} assigned to the CoOOH compound.

Figure 4 (a-c) show typical SEM images at different magnifications of graphene synthesized on the Ni foam substrate showing a porous structure. The SEM images at a high magnification show wrinkles and ripples of graphene sheets which could be attributed to differences in thermal expansion coefficients between graphene and Ni substrate [42]. Figure 4 (d-f) show SEM images at different magnification of CoOOH synthesized on the Ni-FG substrate (CoOOH/Ni-FG). The images at low and high magnifications show homogenous coating of well-ordered intersected nanosheets forming a porous structure.

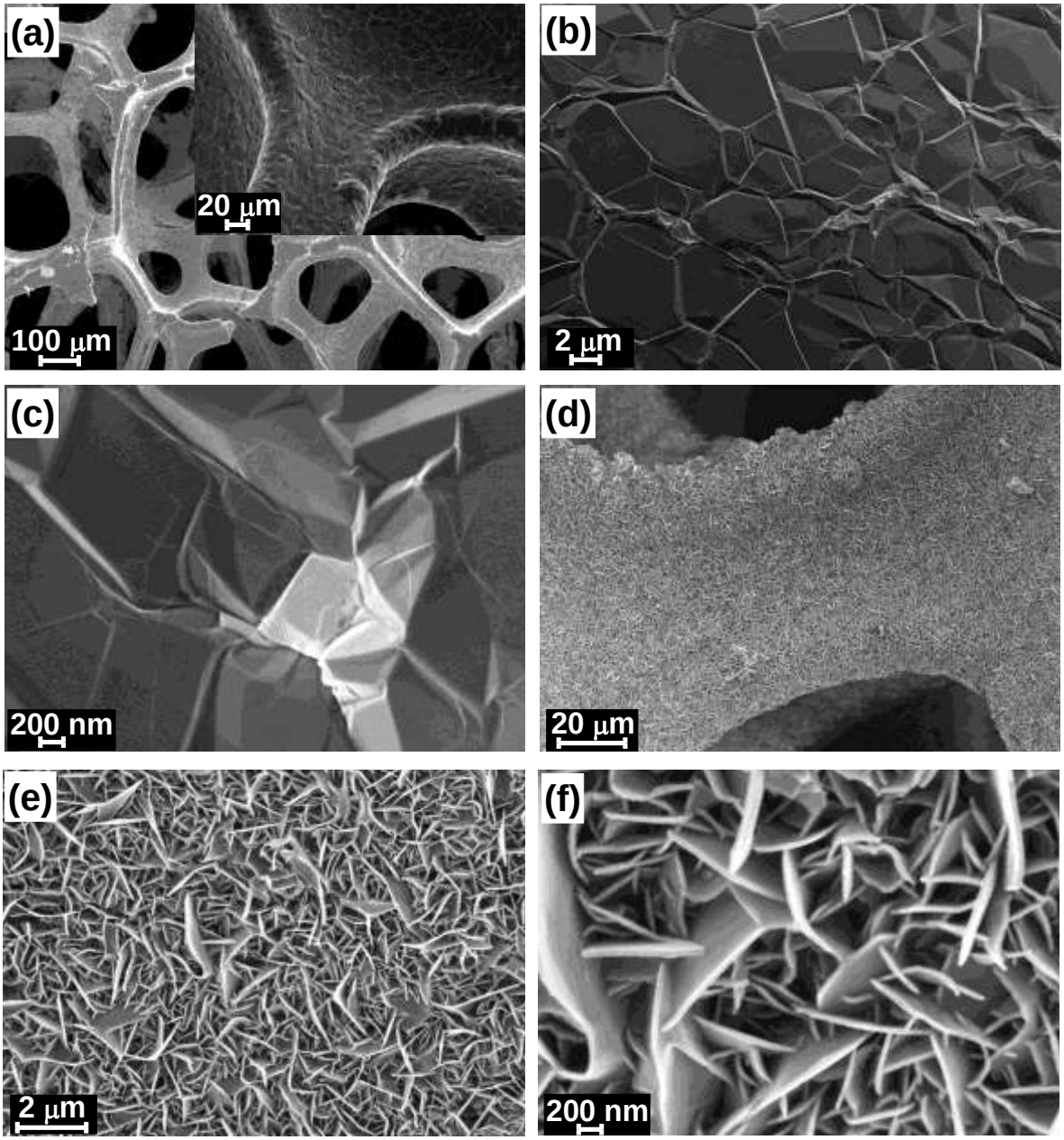

Figure 4 (a) shows a secondary electron beam image showing area 1 and 2 from which the EDX data of the CoOOH/Ni-FG was obtained as shown in figure 5(b). Figure 5(b) shows the presence of C, O, Al, Co and Ni in the sample. Similar to the study of Xu *et al.* [43] and Abushrenta *et al.* [44], a ratio of Co to Al concentration is high and that confirms a successful alkaline etching of the Al cations in CoAl-LDH nanosheets using a NaOH solution for 48 h to give CoOOH nanosheets.

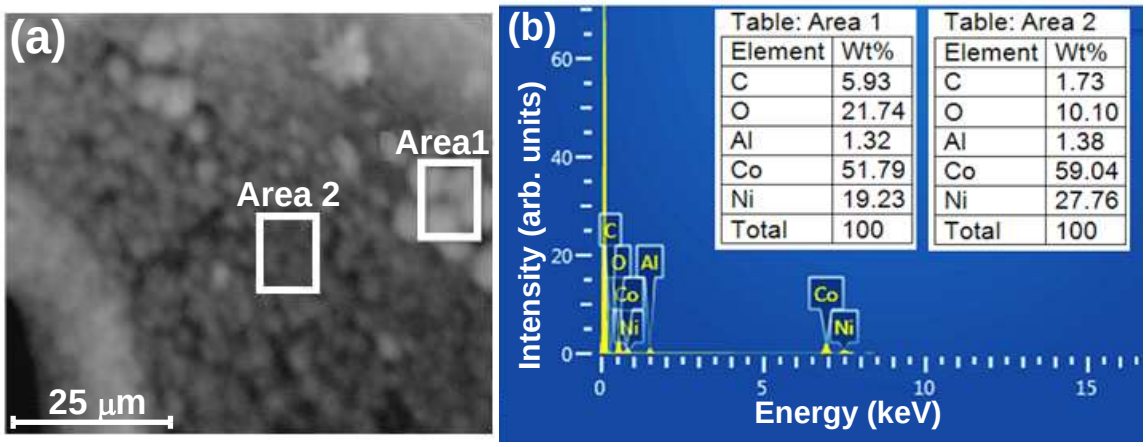

Figure 5: (a) Secondary electron beam image showing area 1 and 2 from which the (b) EDX data of the CoOOH synthesized on the Ni-FG substrate (CoOOH/Ni-FG) was obtained which shows the presence of C, O, Al, Co and Ni in the sample.

5.2 Electrochemical characterization

Figure 6 (a) shows CV curves of Ni-F, Ni-FG, and CoOOH/Ni-FG at a scan rate of 50 mV s^{-1} in a potential range of 0.0 – 0.45 V. CV curves of these electrode materials showing existence of reduction and oxidation peaks. For instance, CV curves of both Ni-F and Ni-FG show peaks that corresponds to the transformation reaction between $Ni(OH)_2$ and NiOOH [45], CV curve of a CoOOH/Ni-FG electrode shows a distinct difference in the current response (showing much higher current response which indicates high capacitance) compared to Ni-F and Ni-FG electrodes at the same potential of 0.45 V, indicating a better electrochemical response. Consequently, further investigation of the capacitive properties of CoOOH/Ni-FG electrode was made. Figure 6 (b) shows the CV curves of the CoOOH/Ni-FG electrode at different scan rates between 5 mV s^{-1} and 50 mV s^{-1}, but in the same potential window. These curves show the redox peaks which could be mainly due to electrochemical surface reactions on the CoOOH material corresponding to cathodic and anodic peaks at ~ 0.1 and ~ 0.37 V vs Ag/AgCl respectively. These redox peaks can be explained by the reversible

electrochemical oxidation and reduction (redox reaction) between Co^{2+} and Co^{3+} expressed as[15,46]

$$CoOOH + OH^- \Leftrightarrow CoO_2 + H_2O + e^- \quad (1)$$

From this redox equation, a theoretical specific value of 1747.9 mAh g^{-1} in 6M KOH electrolyte is deduced. In figure 6 (b), it can be seen that as the scan rate increases, the anodic peak shifts positively whereas the cathodic peak shifts negatively and this shift is attributed to the polarization of the electrodes due to the electrolyte ions diffusion in the porous structure of the electrode during redox reaction at the higher scan rates. The shapes of the curves (showing reduction and oxidation peaks) indicate that the predominant mechanism of charge storage in this material is based on Faradic characteristics [15].

Figure 6 (c) shows the charge-discharge (CD) curves of CoOOH/Ni-FG electrode at current densities of 0.5–10 A g^{-1} in the potential window range of 0.0 V–0.45 V. The curves clearly show two voltage steps, specifically, a fast potential drop in the range of 0.41 V–0.24 V and a slow potential drop in the range of 0.24 V–0.14 V. Similar to CV curves, these voltage drop regions of charge-discharge curves (0.24 V–0.14 V) show Faradic behaviour of the electrode resulting from the electrochemical redox reaction at an interface between electrode and electrolyte[47]. From the CD curves, the specific capacity Q_D of the electrode was calculated using the following expression:

$$Q_D = \frac{I \times t_D}{m \times 3.6} \quad (2)$$

where I is the discharge current (A), t is the discharge time (s), m is the mass of the active material (g), and Q_D is the specific discharge capacity (mAh g^{-1}). The specific capacity of CoOOH/Ni-FG as a function of the current density is shown in figure 6 (d). At a current density of 0.5 A g^{-1}, the specific capacity of the CoOOH/Ni-FG electrode was calculated as

199 mAh g^{-1}. This value is one order of magnitude smaller than the theoretical value and this could be due to the poor crystallinity of the obtained CoOOH material after etching of Al from the CoAl-LDH. Furthermore, poor conductivity of metal oxides and hydroxides, in general can also impede the electrochemical performance of the electrode.

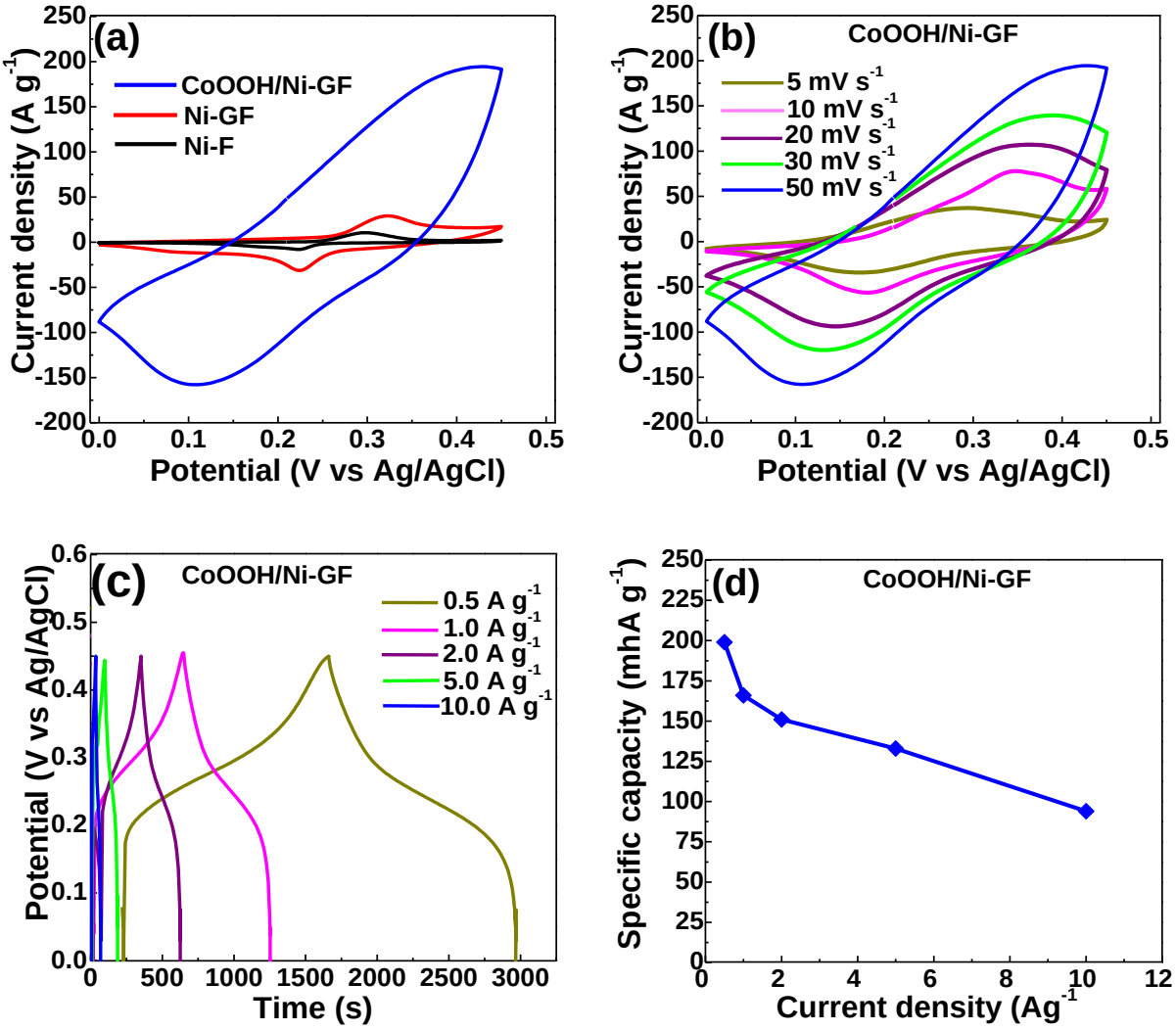

Figure 6: (a) Cyclic voltammetry (CV) of Ni-F, Ni-FG and CoOOH /Ni-FG at a scan rate of 50 mV s^{-1}. (b) CV of CoOOH /Ni-FG at scan rates ranging from 5 to 30 mV s^{-1}. (c) Galvanostatic charge–discharge of CoOOH /Ni-FG at current densities of 0.5 to 10 A g^{-1}. (d) Specific capacity of CoOOH /Ni-FG composite electrode versus current densities.

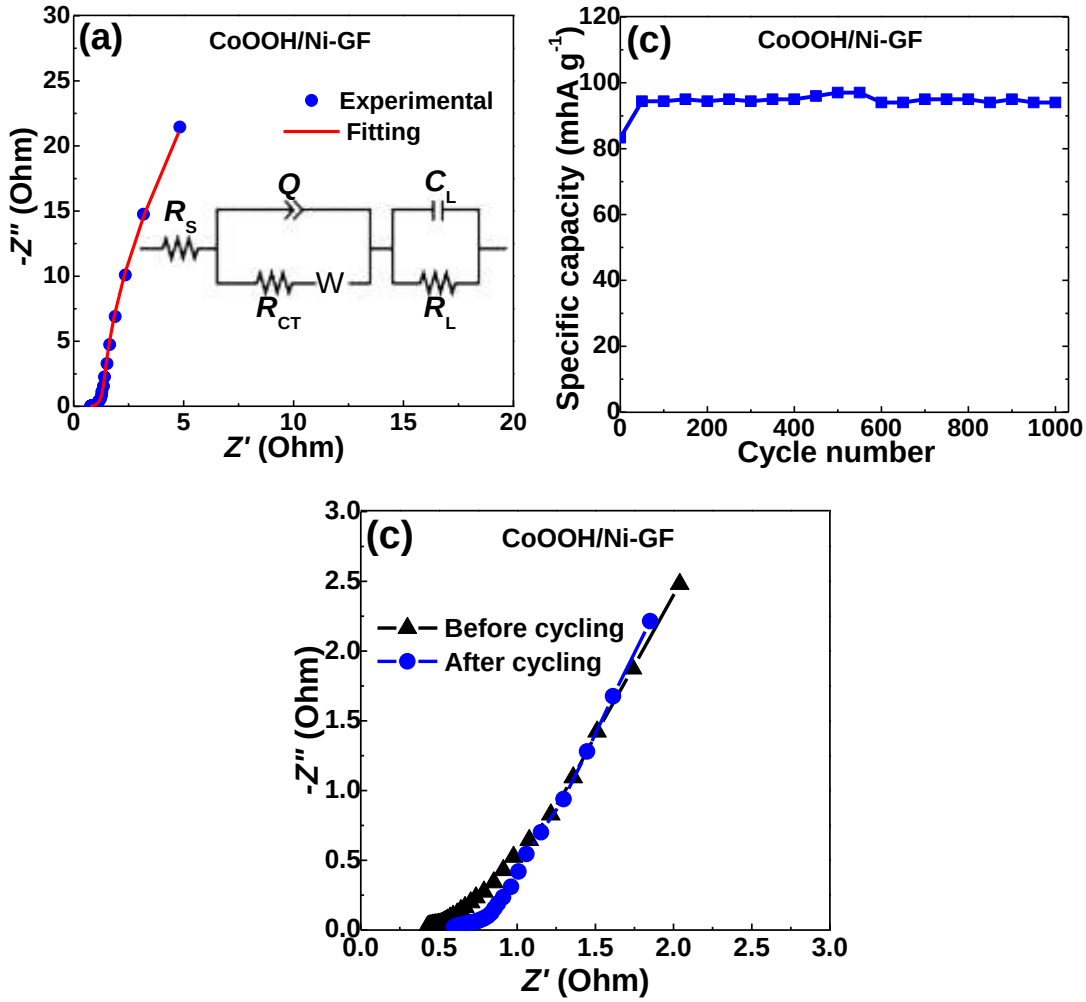

Figure 7: (a) Equivalent circuit (the inset to the figure) fitting to the EIS plot of CoOOH/Ni-FG electrode with ZFIT software that applies the complex nonlinear least-squares (CNLS) method to the equivalent circuit. (b) The dependence of the specific capacity and cycle number at current density of 10 A g^{-1}. (c) Nyquist plots of the CoOOH/Ni-FG electrode before and after 1000 charge–discharge cycles.

Figure 7(a) shows Nyquist plot in the frequency range of 10 mHz to 100 kHz of the CoOOH/Ni-FG electrode obtained from EIS measurements using open circuit potentials (the inset to the figure is the magnified high frequency region of the plot). There are two distinct parts, the high-frequency and low-frequency regions suggesting different electrochemical occurrences during the electrochemical process. EIS measurements were fitted with ZFIT software that applies the complex nonlinear least-squares (CNLS) method to the equivalent circuit (the inset to the figure) as shown in figure 7 (a). Interestingly, the circuit parameters

designate different electrochemical process occurring at the electrode/electrolyte interface. At the high-frequency region, the circuit represents the combined resistance (ionic resistance, intrinsic resistance, and contact resistance) as a result of electrolyte, active material/current collector interactions referred to as solution resistance or equivalent series resistance (R_S). This resistance is estimated from the Nyquist plot by reading the intercept on the x-axis of the high frequency region and is found to be 0.94Ω. At low-frequency region, the circuit represents the Warburg impedance, *W*, due to the diffusion/transport of OH^- ions within the porous structure of the electrode during the redox reactions and indicate the capacitive behavior of the electrode [48]. In addition, the Warburg impedance, *W*, can be expressed as [49]: $W = \frac{A}{j\omega^{0.5}}$, where *A* is the Warburg coefficient, ω is the angular frequency. In the equivalent circuit (the inset to the figure 7 (a)), the solution resistance, R_S, is connected in series to the constant phase element *Q* and the charge transfer resistance R_{CT}. However, R_{CT} and *Q* are connected in parallel to each other forming a circuit which models high-frequency to mid-frequency region of the Nyquist plot and this is attributed to the ideal capacitance of the electrode. The constant phase element *Q*, can be expressed as[50]: $Q = \frac{1}{T(j\omega)^n}$, where *T* is the frequency-independent constant with dimensions of $(F\ cm^{-2})^n$ related to the roughness and pseudocapacitive kinetics of the electrode surface, the values for *n* range from –1 to 1 and can be calculated from the slope of the log *Z* versus log *f*. For values of *n* = 0, *Q* acts as a pure resistor and for *n* = 1, *Q* acts as a pure capacitor and for *n* = –1, *Q* acts as an inductor [51]. Furthermore, at the low frequency region, an ideal electrode yields a vertical line parallel to the imaginary axis with a mass capacitance given by *Q*. The deviation from this ideal behaviour is attributed to the leakage resistance R_L which is connected in parallel to the C_L in the equivalent circuit. C_L denotes the pseudocapacitance which arises due to the Faradaic charge transfer process [49]. The *n*-value obtained from the fitting of the Nyquist

plot for the CoOOH/Ni-FG electrode was 0.91. Therefore, the fitting results for *n* show a capacitive behaviour of the electrode. A summary of the CNLS fitting parameters from the experimental impedance spectra (Figure 7 (a)) is presented in Table 1.

Table1: A summary of the CNLS fitting parameters from the experimental impedance spectra, as shown in Figure 8(b).

R_S (Ω)	R_{CT} (Ω)	C_L (F)	*n*	*Q*
0.94	1.21	1	0.91	1

The cycling stability of the CoOOH/Ni-FG electrode was investigated at a current density of 10 A g^{-1} for 1000 cycles, as shown in figure 7 (b). The CoOOH/Ni-FG electrode shows the specific capacity of 95 mAh g^{-1}at 10.0 A g^{-1} with 98 % capacity retention after 1000 cycles. Nyquist plots (Figure 7 (c)) of the CoOOH/Ni-FG electrode before and after 1000 charge–discharge cycles shows similar curves, suggesting good electrochemical stability of the active material.

5.3. Morphology and structure after electrochemical analysis

The structure of the electrode material after electrochemical measurement is presented to elucidate any structural change or degradation that might have occurred during the cycling process. Figure 8 (a) and (b) show the SEM images (low and high magnifications) of the CoOOH/Ni-FG after electrochemical analysis. These images show a porous structure of nanosheets as seen before electrochemical analysis (Figure 4 (e) and (f)), however, with an effect of electrolyte and this suggest a good stability in the morphology of CoOOH electrode material. It is worth mentioning that these SEM images were acquired using 1 kV beam and the working distance (WD)of 2.5 mm compare to those in figure 4 which were acquired using 2 kV beam and the WD of 2.7 mm. As a result, SEM images in figure 8 (a) and (b) appear larger than those in figure 4 (e) and (f).

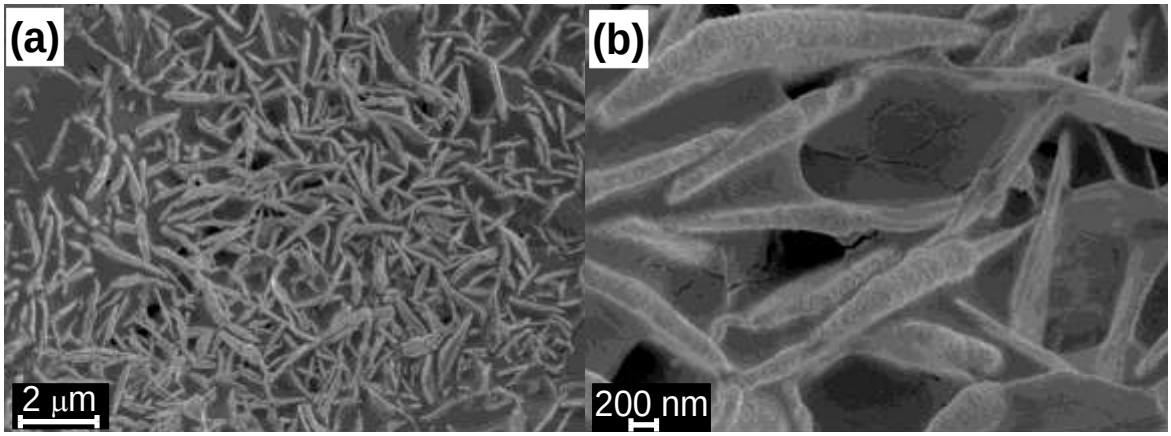

Figure 8: (a) and (b) SEM images (low and high magnifications) of the CoOOH on Ni foam graphene (CoOOH/Ni-FG) after electrochemical analysis showing CoOOH intersected nanosheets covered with dried electrolyte which also filled the space between sheets (porous structure). These SEM images were acquired using 1 kV beam and the working distance of WD = 2.5 mm.

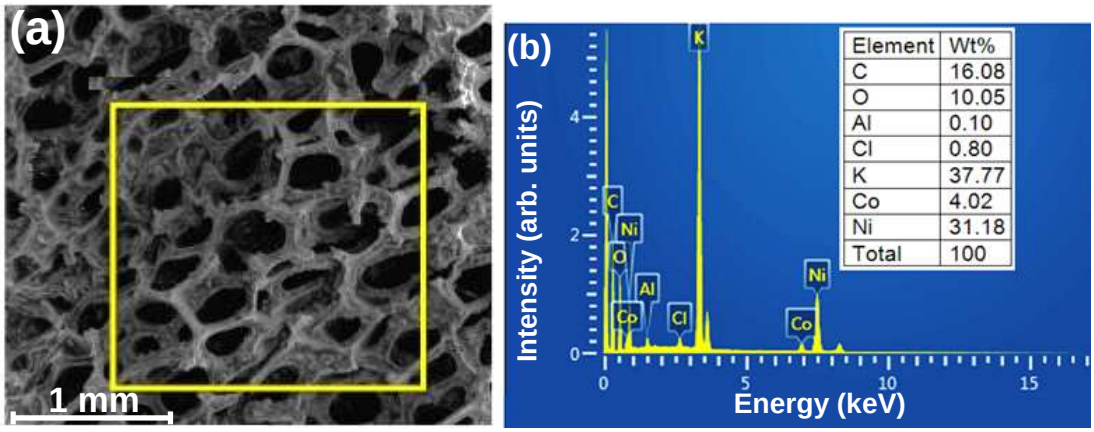

Figure 9: (a) and (b) SEM images (low and high magnifications) of the CoOOH on Ni foam graphene (CoOOH/Ni-FG) after electrochemical analysis showing CoOOH intersected nanosheets covered with dried electrolyte which also filled the space between sheets (porous structure). These SEM images were acquired using 1 kV beam and the working distance of WD = 2.5 mm.

Figure 9 (a) shows a secondary electron beam image showing area from which the EDX data of the CoOOH/Ni-FG after electrochemical analysis was obtained (see figure 9(b)).Figure 9 (b) shows the presence of C, O, Al, Co and Ni in the sample and additional elements due to electrochemical analysis. A high concentration of K confirms the presence or the effect of electrolyte (i.e. KOH) as seen in figure 9(b) after electrochemical analysis. A ratio of Co to Al concentration is still high (as observed before electrochemical analysis in figure 5 and that

confirms structural stability of CoOOH compound. This is further supported by Raman spectra obtained before and after electrochemical analysis which shows similar spectra confirming a good stability in the structure of the CoOOH electrode material and the underlying graphene sheet (see figure 10 (a)). In order to compare our results with other cobalt-based faradic materials, we recalculated the specific capacity from the estimated discharge time and current density from the articles that are being referred to in figure 10 (b) in order to report the realistic values as suggested by Laheäär *et al* [52]. Figure 10 (b) presents a comparison of specific capacity at a current densities of 0.5 to 2.0 A g^{-1} obtained in this work and other previous published reports by Deng *et al.* [32], Zhu *et al.* [9], Nguyen *et al.* [10], Zhao *et al.* [30], Ghosh *et al.* [53] and SengáTan *et al.* [12]. Our results are superior to the previously published Co-based electrode materials for supercapacitor applications.

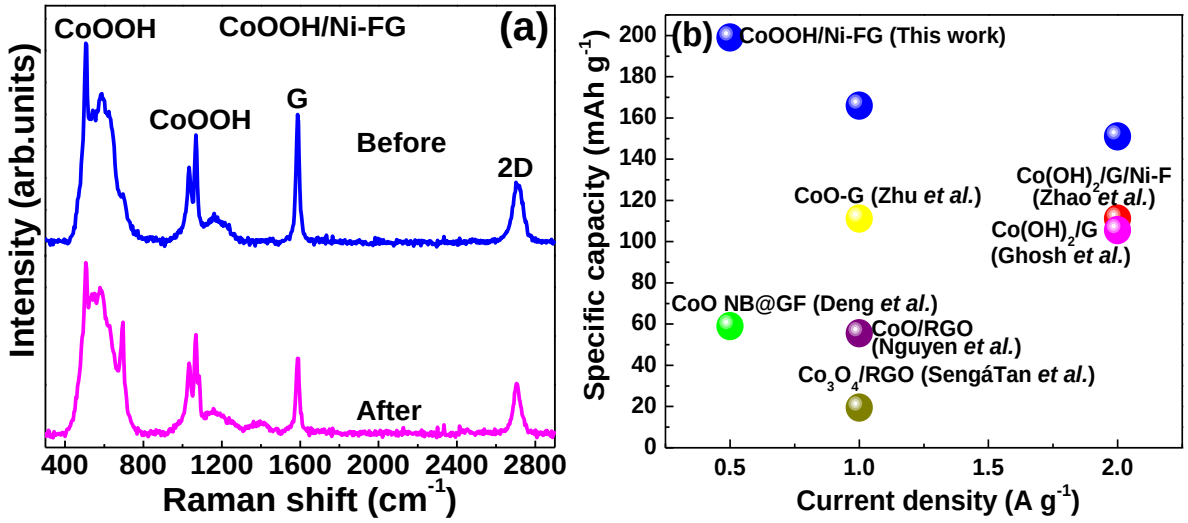

Figure 10: (a) Raman spectra of the CoOOH synthesized on the Ni-FG substrate (CoOOH/Ni-FG) before and after electrochemical analysis. (b) A comparison of specific capacity at a current density of 0.5, 1.0 and 2.0 A g^{-1} obtained in this work and other previous published reports by Deng *et al.* [32], Zhu *et al.* [9], Nguyen *et al.* [10], Zhao *et al.* [30], Ghosh *et al.* [52] and SengáTan *et al.* [12].

6. Conclusion

The morphology of the synthesized CoOOH on the Ni-FG substrate showed a homogenous coating of well-ordered intersected nanosheets showing porous structure. The morphology of synthesized graphene sheet on the Ni foam showed wrinkles and ripples of graphene which retained the advantages of homogeneous adsorption and distribution of CoOOH intersected nanosheets on Ni-FG substrate. The morphology and structural analysis confirmed elemental composition and crystalline structure of the CoOOH compound before and after electrochemical analysis of the electrode. The electrochemical behavior indicated that the CoOOH/Ni-FG electrode is a good Faradic electrode material exhibiting a high specific discharge capacity of 199 mAh g^{-1} at a current density of 0.5 A g^{-1}. In addition ,the supercapacitor also exhibit good cycle stability with a 98 % capacity retention after 1000 cycles. These results suggest that the CooOH/Ni-FG electrode material has great potential as a high capacitiy device and is further expected to contribute significantly to the ongoing scientific reports on Faradaic electrode materials for electrochemical applications.

Acknowledgements

This work is based upon research supported by the South African Research Chairs Initiative of the Department of Science and Technology and National Research Foundation of South Africa (Grant No. 97994). T. M. Masikhwa and M. J. Madito acknowledge financial support from the University of Pretoria and the NRF for their PhD bursaries. A. Bello acknowledges the University of Pretoria's financial support for his Postdoctoral fellowship.

REFERENCES

[1] M. Winter, R.J. Brodd, What are batteries, fuel cells, and supercapacitors?, Chem. Rev. 104 (2004) 4245–4270.

[2] A. Burke, Ultracapacitors: why, how, and where is the technology, J. Power Sources. 91 (2000) 37–50.

[3] J.R. Miller, P. Simon, Fundamentals of Electrochemical Capacitor Design and Operation, Electrochem. Soc. Interface. c (2008) 31–32.

[4] K. Chen, D. Xue, Materials chemistry toward electrochemical energy storage, J. Mater. Chem. A. 4 (2016) 7522–7537.

[5] J. Yan, T. Wei, W. Qiao, B. Shao, Q. Zhao, L. Zhang, et al., Rapid microwave-assisted synthesis of graphene nanosheet/Co_3O_4 composite for supercapacitors, Electrochim. Acta. 55 (2010) 6973–6978.

[6] A.S. Arico, P. Bruce, B. Scrosati, J.-M. Tarascon, W. van Schalkwijk, Nanostructured materials for advanced energy conversion and storage devices, Nat Mater. 4 (2005) 366–377.

[7] H. Wang, H.S. Casalongue, Y. Liang, H. Dai, Ni (OH) 2 nanoplates grown on graphene as advanced electrochemical pseudocapacitor materials, J. Am. Chem. Soc. 132 (2010) 7472–7477.

[8] J. Deng, L. Kang, G. Bai, Y. Li, P. Li, X. Liu, et al., Solution combustion synthesis of cobalt oxides (Co_3O_4 and Co_3O_4/CoO) nanoparticles as supercapacitor electrode materials, Electrochim. Acta. 132 (2014) 127–135.

[9] Y.G. Zhu, Y. Wang, Y. Shi, Z.X. Huang, L. Fu, H.Y. Yang, Phase Transformation Induced Capacitance Activation for 3D Graphene-CoO Nanorod Pseudocapacitor, Adv. Energy Mater. 4 (2014) 1301788.

[10] T.T. Nguyen, R.K. Deivasigamani, D. Kharismadewi, Y. Iwai, J.-J. Shim, others, Facile synthesis of cobalt oxide/reduced graphene oxide composites for electrochemical capacitor and sensor applications, Solid State Sci. 53 (2016) 71-77.

[11] M.Q. Zhao, Q. Zhang, J.Q. Huang, F. Wei, Hierarchical nanocomposites derived from nanocarbons and layered double hydroxides - Properties, synthesis, and applications, Adv. Funct. Mater. 22 (2012) 675–694.

[12] K. SengáTan, C. MingáLi, others, Fabrication of Co_3O_4-reduced graphene oxide scrolls for high-performance supercapacitor electrodes, Phys. Chem. Chem. Phys. 13 (2011) 14462–14465.

[13] K. Chen, C. Sun, D. Xue, Morphology engineering of high performance binary oxide electrodes, Phys. Chem. Chem. Phys. 17 (2015) 732–750.

[14] P. Lu, F. Liu, D. Xue, H. Yang, Y. Liu, Phase selective route to $Ni(OH)_2$ with enhanced supercapacitance: Performance dependent hydrolysis of Ni (Ac) 2 at hydrothermal conditions, Electrochim. Acta. 78 (2012) 1–10.

[15] L. Zhu, W. Wu, Y. Zhu, W. Tang, Y. Wu, Composite of CoOOH nanoplates with multiwalled carbon nanotubes as superior cathode material for supercapacitors, J. Phys. Chem. C. 119 (2015) 7069–7075.

[16] A.D. Jagadale, D.P. Dubal, C.D. Lokhande, Electrochemical behavior of potentiodynamically deposited cobalt oxyhydroxide (CoOOH) thin films for supercapacitor application, Mater. Res. Bull. 47 (2012) 672–676.

[17] M. Wang, W. Ren, Y. Zhao, H. Cui, Synthesis of nanostructured CoOOH film with high electrochemical performance for application in supercapacitor, J. Nanoparticle Res. 16 (2014) 1–7.

[18] A. Davies, A. Yu, Material advancements in supercapacitors: from activated carbon to carbon nanotube and graphene, Can. J. Chem. Eng. 89 (2011) 1342–1357.

[19] D. Antiohos, M. Romano, J. Chen, J.M. Razal, Carbon Nanotubes for Energy Applications, (n.d.).

[20] M. Zhi, C. Xiang, J. Li, M. Li, N. Wu, Nanostructured Carbon-Metal Oxide Composite Electrodes for Supercapacitors: Review, Nanoscale.5 (2012) 72–88.

[21] H. Jiang, J. Ma, C. Li, Mesoporous carbon incorporated metal oxide nanomaterials as supercapacitor electrodes, Adv. Mater. 24 (2012) 4197–4202.

[22] K. Chen, D. Xue, In-situ electrochemical route to aerogel electrode materials of graphene and hexagonal CeO 2, J. Colloid Interface Sci. 446 (2015) 77–83.

[23] Z. Yang, S. Chabi, Y. Xia, Y. Zhu, Preparation of 3D graphene-based architectures and their applications in supercapacitors, Prog. Nat. Sci. Mater. Int. 25 (2015) 1–9.

[24] X. Fan, X. Chen, L. Dai, 3D graphene based materials for energy storage, Curr. Opin. Colloid Interface Sci. 20 (2015) 429–438.

[25] A. Bello, K. Makgopa, M. Fabiane, D. Dodoo-Ahrin, K.I. Ozoemena, N. Manyala, Chemical adsorption of NiO nanostructures on nickel foam-graphene for supercapacitor applications, J. Mater. Sci. 48 (2013) 6707–6712.

[26] M.T. Pettes, H. Ji, R.S. Ruoff, L. Shi, Thermal transport in three-dimensional foam architectures of few-layer graphene and ultrathin graphite, Nano Lett. 12 (2012) 2959–2964.

[27] K. Chen, D. Xue, Rare earth and transitional metal colloidal supercapacitors, Sci. China Technol. Sci. 58 (2015) 1768–1778.

[28] K. Chen, Y. Yang, K. Li, Z. Ma, Y. Zhou, D. Xue, CoCl2 designed as excellent pseudocapacitor electrode materials, ACS Sustain. Chem. Eng. 2 (2013) 440–444.

[29] X.C. Dong, H. Xu, X.W. Wang, Y.X. Huang, M.B. Chan-Park, H. Zhang, et al., 3D graphene-cobalt oxide electrode for high-performance supercapacitor and enzymeless glucose detection, ACS Nano. 6 (2012) 3206–3213.

[30] C. Zhao, X. Wang, S. Wang, Y. Wang, Y. Zhao, W. Zheng, Synthesis of Co (OH) $_2$/graphene/Ni foam nano-electrodes with excellent pseudocapacitive behavior and high cycling stability for supercapacitors, Int. J. Hydrogen Energy. 37 (2012) 11846–11852.

[31] J.-J. Shim, others, The 3D Co $_3$ O $_4$/graphene/nickel foam electrode with enhanced electrochemical performance for supercapacitors, Mater. Lett. 139 (2015) 377–381.

[32] W. Deng, Y. Sun, Q. Su, E. Xie, W. Lan, Porous CoO nanobundles composited with 3D graphene foams for supercapacitors electrodes, Mater. Lett. 137 (2014) 124–127.

[33] Z. Lu, W. Zhu, X. Lei, G.R. Williams, D. O'Hare, Z. Chang, et al., High pseudocapacitive cobalt carbonate hydroxide films derived from CoAl layered double hydroxides, Nanoscale. 4 (2012) 3640.

[34] L.M. Malard, M. a. Pimenta, G. Dresselhaus, M.S. Dresselhaus, Raman spectroscopy in graphene, Phys. Rep. 473 (2009) 51–87.

[35] A.C. Ferrari, J.C. Meyer, V. Scardaci, C. Casiraghi, M. Lazzeri, F. Mauri, et al., Raman Spectrum of

Graphene and Graphene Layers, Phys. Rev. Lett. 97 (2006) 187401.

[36] M.J. Madito, A. Bello, J.K. Dangbegnon, C.J. Oliphant, W.A. Jordaan, T.M. Masikhwa, et al., Raman analysis of bilayer graphene film prepared on commercial Cu(0.5 at% Ni) foil, J. Raman Spectrosc. (2015).

[37] A. Reina, S. Thiele, X. Jia, S. Bhaviripudi, M.S. Dresselhaus, J.A. Schaefer, et al., Growth of large-area single- and Bi-layer graphene by controlled carbon precipitation on polycrystalline Ni surfaces, Nano Res. 2 (2009) 509–516.

[38] W. Liu, S. Kraemer, D. Sarkar, H. Li, P.M. Ajayan, K. Banerjee, Controllable and rapid synthesis of high-quality and large-area bernal stacked bilayer graphene using chemical vapor deposition, Chem. Mater. 26 (2014) 907–915.

[39] N. Liu, L. Fu, B. Dai, K. Yan, X. Liu, R. Zhao, et al., Universal Segregation Growth Approach to Wafer-Size Graphene from Non-Noble Metals, Nano Lett. 11 (2011) 297–303.

[40] J. Yang, H. Liu, W.N. Martens, R.L. Frost, Synthesis and Characterization of Cobalt Hydroxide, Cobalt Oxyhydroxide, and Cobalt Oxide Nanodiscs, J. Phys. Chem. C. 114 (2010) 111–119.

[41] T. Pauporté, L. Mendoza, M. Cassir, M.C. Bernard, J. Chivot, Direct Low-Temperature Deposition of Crystallized CoOOH Films by Potentiostatic Electrolysis, J. Electrochem. Soc. 152 (2005) C49. doi:10.1149/1.1842044.

[42] C. Mattevi, H. Kim, M. Chhowalla, A review of chemical vapour deposition of graphene on copper, J. Mater. Chem. 21 (2011) 3324.

[43] T. Xu, X. Wu, Y. Li, W. Xu, Z. Lu, Y. Li, et al., Morphology and Phase Evolution of CoAl Layered Double Hydroxides in an Alkaline Environment with Enhanced Pseudocapacitive Performance, ChemElectroChem. 2 (2015) 679–683.

[44] N. Abushrenta, X. Wu, J. Wang, J. Liu, X. Sun, Hierarchical Co-based Porous Layered Double Hydroxide Arrays Derived via Alkali Etching for High-performance Supercapacitors, Sci. Rep. 5 (2015) 13082.

[45] L. Zhang, J. Wang, J. Zhu, X. Zhang, K. San Hui, K.N. Hui, 3D porous layered double hydroxides

grown on graphene as advanced electrochemical pseudocapacitor materials, J. Mater. Chem. A. 1 (2013) 9046–9053.

[46] K.K. Lee, W.S. Chin, C.H. Sow, Cobalt-based compounds and composites as electrode materials for high-performance electrochemical capacitors, J. Mater. Chem. A. 2 (2014) 17212–17248.

[47] D.-D. Zhao, S.-J. Bao, W.-J. Zhou, H.-L. Li, Preparation of hexagonal nanoporous nickel hydroxide film and its application for electrochemical capacitor, Electrochem. Commun. 9 (2007) 869–874.

[48] T.M. Masikhwa, J.K. Dangbegnon, A. Bello, M.J. Madito, D. Momodu, N. Manyala, Preparation and electrochemical investigation of the cobalt hydroxide carbonate/activated carbon nanocomposite for supercapacitor applications, J. Phys. Chem. Solids. 88 (2016) 60–67.

[49] Y. Zhou, H. Xu, N. Lachman, M. Ghaffari, S. Wu, Y. Liu, et al., Advanced asymmetric supercapacitor based on conducting polymer and aligned carbon nanotubes with controlled nanomorphology, Nano Energy. 9 (2014) 176–185.

[50] F. Tao, Y.Q. Zhao, G.Q. Zhang, H.L. Li, Electrochemical characterization on cobalt sulfide for electrochemical supercapacitors, Electrochem. Commun. 9 (2007) 1282–1287.

[51] B.E. Conway, Conway, B. E. Electrochemical Supercapacitors: Scientific Fundamentals and Technological Applications;, Kluwer Academic/ Plenum, New York, 1999.

[52] a. Lahe????r, P. Przygocki, Q. Abbas, F. B??guin, Appropriate methods for evaluating the efficiency and capacitive behavior of different types of supercapacitors, Electrochem. Commun. 60 (2015) 21–25.

[53] D. Ghosh, S. Giri, C.K. Das, Preparation of CTAB-assisted hexagonal platelet Co (OH) 2/graphene hybrid composite as efficient supercapacitor electrode material, ACS Sustain. Chem. Eng. 1 (2013) 1135–1142.